Multiple Fates of Newly Synthesized Neurofilament Proteins: Evidence for a Stationary Neurofilament Network Distributed Nonuniformly along Axons of Retinal Ganglion Cell Neurons

Ralph A. Nixon*‡ and Kimberly B. Logvinenko*

*Ralph Lowell Laboratories, Mailman Research Center, McLean Hospital, Belmont, Massachusetts 02178; ‡Department of Psychiatry and Program in Neuroscience, Harvard Medical School, Boston, Massachusetts 02115

Abstract. We have studied the fate of neurofilament proteins (NFPs) in mouse retinal ganglion cell (RGC) neurons from 1 to 180 d after synthesis and examined the proximal-to-distal distribution of the newly synthesized 70-, 140-, and 200-kD subunits along RGC axons relative to the distribution of neurofilaments. Improved methodology for intravitreal delivery of [^{3}H]proline enabled us to quantitate changes in the accumulation and subsequent decline of radiolabeled NFP subunits at various postinjection intervals and, for the first time, to estimate the steady state levels of NFPs in different pools within axons.

Two pools of newly synthesized triplet NFPs were distinguished based on their kinetics of disappearance from a 9-mm "axonal window" comprising the optic nerve and tract and their temporal-spatial distribution pattern along axons. The first pool disappeared exponentially between 17 and 45 d after injection with a half-life of 20 d. Its radiolabeled wavefront advanced along axons at 0.5–0.7 mm/d before reaching the distal end of the axonal window at 17 d, indicating that this loss represented the exit of neurofilament proteins composing the slowest phase of axoplasmic transport (SCa or group V) from axons. About 32% of the total pool of radiolabeled neurofilament proteins, however, remained in axons after 45 d and disappeared exponentially at a much slower rate ($t_{1/2}$ = 55 d). This second NFP pool assumed a nonuniform distribution along axons that was characterized proximally to distally by a 2.5-fold gradient of increasing radioactivity. This distribution pattern did not change between 45 and 180 d indicating that neurofilament proteins in the second pool constitute a relatively stationary structure in axons. Based on the relative radioactivities and residence time (or turnover) of each neurofilament pool in axons, we estimate that, in the steady state, more neurofilament proteins in mouse RGC axons may be stationary than are undergoing continuous slow axoplasmic transport. This conclusion was supported by biochemical analyses of total NFP content and by electron microscopic morphometric studies of neurofilament distribution along RGC axons. The 70-, 140-, and 200-kD subunits displayed a 2.5-fold proximal to distal gradient of increasing content along RGC axons. Neurofilaments were more numerous at distal axonal levels, paralleling the increased content of NFP.

We conclude that the neurofilament lattice in mouse RGC axons is nonuniform along its length, and that a significant portion of the neurofilament network in these axons is relatively stationary and maintained by neurofilament proteins that are deposited nonuniformly along axons during slow axoplasmic transport.

NEUROFILAMENTS, the intermediate filaments of neurons, constitute a major component of the neuronal cytoskeleton. Together with microtubules, neurofilaments form a cross-linked latticework that supports the nerve cell and helps define its shape (15, 22). In axons, the neurofilament network appears to be a major intrinsic determinant of axonal diameter (16, 22) and to confer a degree of stability on the neurite once the neuron matures (23, 28).

The content of neurofilaments along axons is controlled largely by the axonal transport of neurofilament proteins (NFPs)[1] (16, 22). Still unclear, however, is the form(s) in which neurofilament proteins are transported and the sequence of steps leading to the integration of neurofilaments into the axonal cytoskeleton (49). The coordinate movement of these polypeptides, together with tubulin subunits in some systems (21), has suggested a model in which NFPs are assembled before transport into a neurofilament-microtubule network that is continuous from the cell body to the terminal

[1] *Abbreviations used in this paper*: NFP, neurofilament protein; RGC, retinal ganglion cell.

regions of the axon (21, 22). This proposed network is continuously elaborated from newly synthesized polypeptides in the perikaryon and disassembled in the terminals (21). According to this model, if NFPs were pulse-radiolabeled, they would be expected to advance as a symmetrical wave that resists spreading along its course. Since the network is in constant motion, constituents of the wave would not be deposited in axons. In the steady state, a uniform distribution of NFPs along axons would therefore be expected. By an alternative model (31, 49), NFPs, predominantly as preassembled neurofilaments, move down the axon as precursors to a relatively stationary neurofilament lattice. This model predicts that some of the labeled neurofilaments or NFPs in the moving wave would be deposited along axons as reflected by spreading of the moving wave. If the rate of deposition or turnover of NFPs varied at different axonal sites, a nonuniform distribution of deposited NFPs along the length of axons might be expected.

To evaluate these models experimentally, we studied the fate of NFP subunits in mouse RGC axons from 1 to 180 d after synthesis and examined the axonal distribution of newly synthesized NFPs relative to that of total neurofilament proteins and neurofilaments along the optic pathway. The axoplasmic transport studies focused on several aspects of neurofilament protein translocation and metabolism that have not been extensively investigated. For example, the small size of the mouse optic pathway facilitated analyses of proteins retained along the entire length of axons long after radiolabeled proteins in the slow phases of axoplasmic transport should have reached synaptic terminals. Variation among animals at each postinjection timepoint was reduced by precisely controlling the delivery of radiolabeled amino acids to the retina. As a result, we could reliably compare the absolute radioactivity of a particular axonal protein in animals killed at different timepoints and, thereby, establish the kinetics of NFP disappearance from axons. This additional information allowed us, for the first time, to estimate the size of different axonal neurofilament pools in vivo using data from pulse-radiolabeled NFPs. These data proved to be critical for interpreting conventional pulse-label analyses of NFP behavior during axoplasmic transport.

We observed that newly synthesized NFPs contribute to two pools in retinal ganglion cell (RGC) axons, one consisting of continually moving elements conveyed by axoplasmic transport and the second comprising a relatively stationary phase that is retained in axons and distributed nonuniformly along their lengths. Although the radioactivity associated with the pool of stationary NFPs was half as great as that in the moving pool, its residence time (half-life) in axons was nearly threefold longer. We estimate, therefore, that the stationary pool of NFPs constitutes the greater contribution to the axonal cytoskeleton under steady state conditions. This conclusion is supported by morphometric studies showing a proximal to distal increase in the number of neurofilaments along RGC axons that parallels the distribution of the retained pool of radiolabeled NFPs. We interpret these data to indicate that a substantial portion of the neurofilament network in mouse RGC axons is relatively stationary and is maintained by axonally transported neurofilaments or neurofilament polypeptides that are deposited nonuniformly along axons. The observation that the neurofilament network in RGC axons is nonuniform along its length extends earlier evidence that the axonal cytoskeleton is regionally specialized (4, 35, 36).

Portions of this work have been described in preliminary form (34, 38).

Materials and Methods

Isotope Injections

Male or female mice of the C57Bl/6j strain, aged 10–14 wk at the time of injection, were used in all experiments. Mice were housed at 23°C on a 12-h light-dark cycle. Intravitreal injections of radiolabeled amino acids into anesthetized mice were made with a glass micropipette apparatus as previously described (30). 25 μCi of L-[2,3-^{3}H]proline (specific activity, 30–50 Ci/mmol), purchased from New England Nuclear (Boston, MA), was administered in a volume of 0.20 μl of phosphate-buffered saline, pH 7.4. The following additional measures were taken in studies on the kinetics of NFP disappearance to reduce variation in amounts of radiolabeled amino acid incorporated into axonal proteins in different animals. For a single experiment involving 80–100 mice, identical volumes of labeled precursor solution were injected into all animals within a single 4-h period using calibrated micropipettes. Repeated experiments were carried out at the same time of day to avoid possible circadian effects on protein synthesis or transport. To reduce the risk of leakage from the injection site, the bore of the micropipette tip (70 μm) and the site and depth of the injection were standardized. A given animal was not analyzed as part of the series if leakage of the solution out of the eye was observed.

Tissue Preparation

Mice were killed by cervical dislocation followed by decapitation. After the brain was cooled for several minutes in aluminum foil on ice, the optic nerve and optic tract were freed from the meninges, and the optic tract on each side was severed at a point 2.5-mm from the superior colliculus. This dissected segment, referred to as the primary optic pathway, was 9 mm long and consisted of the optic nerve severed at the scleral surface of the eye, the optic chiasm, and a length of optic tract extending to, but not including, terminals in the lateral geniculate nucleus. Preliminary histological studies of transverse sections of the optic pathway and skip-serial transverse sections of the brain indicated that the analyzed portion of the optic tract remains as a well-defined fiber bundle, which is easily freed from contaminating brain parenchyma during dissection. In some experiments, the optic pathway was cut into consecutive 1.1-mm segments on a micrometer-calibrated slide. Postmortem changes in protein composition were negligible during dissection and analysis (35).

PAGE

One-dimensional SDS PAGE analysis of the tissues was performed by the procedure of Laemmli (19) on 320 mm slab gels using 4–7 or 5–15% linear polyacrylamide gradients (36). Two-dimensional gels were prepared using the general procedure of O'Farrell (40) modified as previously described (5).

Quantitation of Radioactivity

In the initial experiments, radiolabeled proteins on gels were first detected by fluorography (35) and selected bands were cut from the gels. In most experiments, protein bands were cut directly from gels stained with Coomassie Brilliant Blue but not subjected to fluorography. NFPs were identified on gels by comparison with the migration of cytoskeletal proteins from fractions prepared by the method of axonal flotation (26). The radioactivity in gel slices (disintegrations per minute) was determined as previously described (36).

Immunoblot Analyses of NFPs

Antibodies to NFPs, including monospecific polyclonal antibodies to the 200-, 140-, and 70-kD subunits, were generously provided by Dr. Charles Marotta. These have been previously characterized (3, 18). A monoclonal antibody to intermediate filament proteins (41) which cross-reacts with the NFP triplet, was also tested. PAGE-separated proteins from either optic nerve homogenates or cytoskeletal protein preparations were transferred to nitrocellulose membranes. The transferred proteins were immunostained by means of a horseradish peroxidase–conjugated indirect antibody procedure (3).

Quantitation of Total NFP and Total Protein

The total content of each of the three neurofilament subunits in different regions of the optic pathway was measured using a method (33) based upon the quantitative binding of Coomassie Blue dye to proteins (2). NFPs and selected other proteins were cut from gels stained with Coomassie Blue. After quantitatively extracting the dye from the gel slices in methanol, the absorbance

was measured spectrophotometrically at 585 nm. Absorbance readings obtained from blank regions of gel of appropriate area, reflecting nonspecific background, were subtracted from the value for each stained band. The absorbance was linearly related to the protein content for a given protein within the range of weights used in this study. Since dye-binding capacity for different proteins varies, the content of each NFP subunit in consecutive segments of the optic pathway was expressed in relative terms. The increase in NFP content with increasing distance from the eye was studied using simple regression methods. Individual determinations at each distance along the pathway were used in this calculation. Relative protein content was regressed against optic pathway segment, and the hypothesis of a zero slope was tested using a standard two-sided *t*-test (8). Total protein content in tissue samples was determined by the method of Lowry et al. (27).

Electron Microscopy

Mice were anesthetized using ethyl ether and perfused through the heart with 1.5% paraformaldehyde and 1% glutaraldehyde in 0.1 M phosphate buffer (pH 7.3) at room temperature. After the brains were stored overnight at 4°C, the optic pathways were dissected, postfixed with 1% osmium tetroxide in 0.1 M cacodylate buffer, dehydrated through a series of graded alcohols, infiltrated with propylene oxide, and embedded in Poly-bed 812 (Polysciences, Inc., Warrington, PA). Ultra-thin sections stained with 1% aqueous uranyl acetate and 1% lead citrate were examined with a JEOL model S100 electron microscope.

Quantitation of Axonal Neurofilaments and Microtubules

Optic pathways from three animals perfused as described above were cut in transverse section at three levels—1, 4, and 7 mm from the eye—representing proximal, middle, and distal regions of RGC axons, respectively. At each level, a total of 200–280 axons was selected randomly from the population of axonal profiles in which neurofilaments and microtubules appeared in exact cross-section throughout the axoplasm. Axons were chosen equally from the four quadrants of the optic pathway section. The number of axons selected of a particular caliber approximated the relative contribution of this sized fiber to the total axoplasmic area in the optic pathway cross-section. The latter information was obtained from analyses of axonal caliber distributions at each of three optic pathway levels studied. Neurofilaments and microtubules were easily distinguished and counted visually from photographs printed at a final magnification of 75,000. Because of the selection criteria, the frequency of obliquely cut neurofilaments and microtubules was low; these were counted only if they could be unequivocally identified. All counts were performed on randomly assorted photomicrographs by a single observer. Neurofilaments in the same axon counted on separate occasions varied by <5%. A total of 58,509 neurofilaments were counted in 672 axons at the three levels.

The cross-sectional area of each axon analyzed was then measured as described below. The variation in repeated caliber determinations on the same axon was <2%. The number of neurofilaments or microtubules per square micrometer of cross-sectional area of axoplasm, referred to as neurofilament or microtubule density, was then calculated from these data. Regression methods were used to investigate the relationship between the number of neurofilaments and the total axonal area at proximal, middle, and distal axonal levels separately. These relationships were also tested after the number of neurofilaments and axonal area were re-expressed on the logarithm scale to ensure that the assumptions of linear regression were satisfied and, in particular, that the most extreme values did not disproportionately influence the regression coefficients. Tests of the equality of the slopes of the resultant regression lines was performed using a partial F test (8).

Measurement of Axon Calibers

To determine the distributions of axonal calibers at proximal, middle, and distal levels of the optic pathway, 8–12 nonoverlapping fields, each containing ~500 axons were selected equally from the four quadrants of the optic pathway cross-section at each level. The fields were photographed and printed at a final magnification of 6,000. Axonal areas were measured from the prints using a Summagraphics Supergrid digitizer interfaced with a Perkin-Elmer 3220 computer (Perkin-Elmer Corp., Oceanport, NJ). All myelinated axons in a given field were measured unless they were clearly cut in oblique section. The number of excluded axons was 10–12% at each level. The percentage of axons in each of a series of equally spaced size categories was determined at the three levels of each optic pathway. Histograms were constructed by plotting these percentages as a function of axonal caliber. A total of 2,700–3,000 axons from two animals was counted at each level. A two-sample Kolmogorov-Smirnov test (10) was used to compare the distributions of axon calibers at the three levels.

Results

NFPs in RGC Axons

The NFP triplet in the mouse primary optic pathway consists of major 70-, 140-, and 200-kD components (Fig. 1) (2). These subunits were completely separated from other potentially contaminating proteins by one-dimensional SDS PAGE on 320-mm slab gels when gradients of acrylamide at low concentrations (3–7%) were used. Although the two larger NFPs displayed size microheterogeneity (25, 35), the micro-

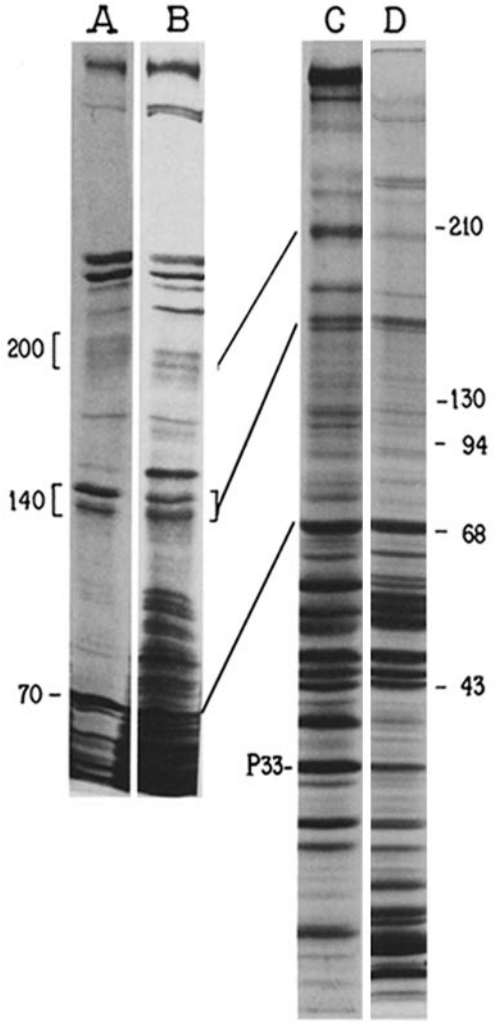

Figure 1. SDS gels of proteins of the mouse optic pathway and radiolabeled proteins comprising the slow phases of axoplasmic transport in RGC neurons. Optic pathways were obtained 6 d after mice were injected intravitreally with [^{3}H]proline. Lane *A*, representing the electrophoretic pattern after fluorography, shows the major cytoskeletal proteins in RGC axons prepared from radiolabeled optic pathways by the method of Chiu and Norton (7). Lane *B* illustrates radiolabeled protein constituents of the SCa (group V) and SCb (group IV) phases of axoplasmic transport. These gels contained 3–7% acrylamide gradients. Lane *C* shows the fluorogram of proteins similar to those in lane *B* separated in gels containing a 5–15% acrylamide gradient. Total proteins of the optic pathway were visualized by Coomassie Brilliant Blue staining of a similar gel (lane *D*). Molecular masses (in thousands) of protein standards electrophoresed in adjacent lanes are given. NFPs are indicated at 200, 140, and 70 kD, and the position of protein 33 (33 kD) is shown. Microheterogeneous forms of the 200- and 140-kD subunits are resolved in these gels.

heterogeneous forms that composed each major subunit were considered together in this study.

Radiolabeled and unlabeled proteins corresponding to the molecular weights of the neurofilament triplet proteins were highly enriched in Triton-insoluble preparations of cytoskeletal proteins (Figs. 1, lane *A*, and 2, lanes *F* and *G*). The 70-, 140-, and 200-kD proteins from optic pathways cross-reacted with polyclonal antibodies against the 70-, 140-, and 200-kD NFP subunits, respectively (Fig. 2, lanes *B–D*). Electroblots of the three proteins from either cytoskeletal protein preparations of optic pathway or unfractionated tissue also immunostained with a monoclonal antibody specific for intermediate filament proteins of all classes (41) (Fig. 2, lanes *E–H*). In addition, when glial cells of the optic pathway were selectively radiolabeled in vitro, no labeled proteins migrated to the same position on gels as the 70- and 140-kD NFPs, and only minor labeling of glial protein(s) at the position of the 200-kD NFP subunit was observed (32). Therefore, glial incorporation of radioactive proline released from axonal proteins or diffusing from the eye after intravitreal injection could not account for the presence of labeled proteins in gel regions containing the NFPs.

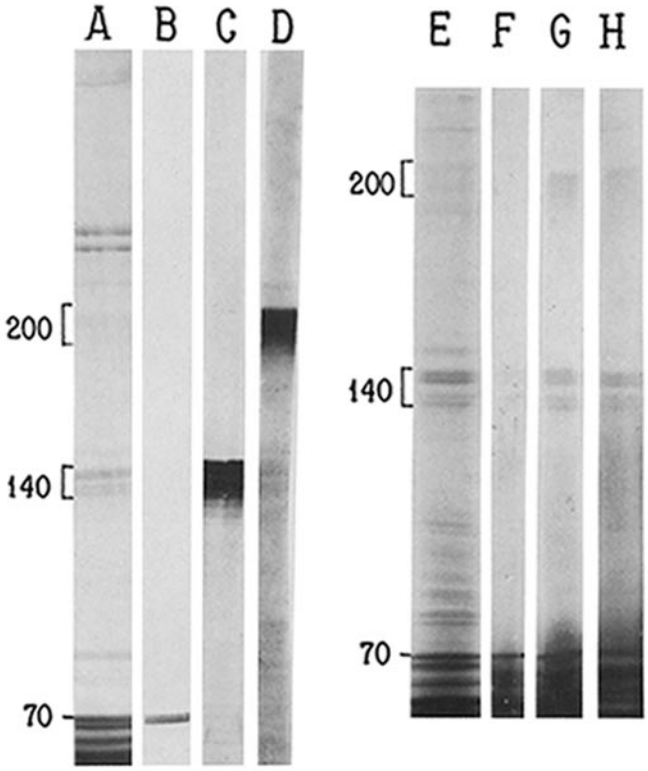

Figure 2. Immunological identification of NFPs. Mouse optic pathways or cytoskeletal proteins from this tissue prepared by the method of Chiu and Norton (7) were subjected to SDS PAGE (4–7% acrylamide gradient). After electrophoresis, proteins were electroblotted onto nitrocellulose and immunostained as described in Materials and Methods. Before electroblotting, an adjacent strip cut from each gel was stained with Coomassie Brilliant Blue. Identical lanes of optic pathway proteins were analyzed as follows: lane *A*, Coomassie Blue; lane *B*, polyclonal anti-rat 70-kD NFP; lane *C*, polyclonal anti-rat 140-kD NFP; lane *D*, polyclonal anti-rat 200-kD NFP. Total proteins (lanes *E* and *H*) or cytoskeletal proteins (lanes *F* and *G*) of the optic pathway were stained with monoclonal antibody to all classes of intermediate filaments (41). Lane *F* was underloaded with protein to improve visualization of the 70-kD subunit. The positions of the three NFP subunits are indicated.

Axoplasmic Transport and Half-lives of NFP Pools

The fate of newly synthesized NFPs in RGC axons was studied by two experimental approaches, the first involving analysis of protein movement through a standard length of axon, and the second involving analysis of the distribution of polypeptides along axons at different times during axoplasmic transport. By the first approach, a 9-mm length of the mouse optic pathway, extending from the proximal optic nerve to the distal optic tract, was chosen as the standard "axonal window." The rate at which NFPs enter and exit this axonal compartment reflects primarily their axoplasmic transport rate. In addition, if the initial specific radioactivity of NFPs synthesized in RGC perikarya is similar in groups of mice allowed to survive for different postinjection intervals, it is possible not only to establish precise transport kinetics, but also to quantitate the proportion of NFPs retained in axons longer than would be predicted from their axoplasmic transport rates. In these experiments, variation in the intravitreal delivery of radiolabeled amino acid among groups of injected mice was reduced sufficiently to permit these additional analyses.

Two groups of 80–100 mice injected intravitreally with [^{3}H]proline were allowed to survive from 1 to 168 d after injection. Changes in the radioactivity associated with the neurofilament triplet proteins and other proteins in the 9-mm optic pathway segment after SDS PAGE were quantitated in each of 8–16 mice per time point. Radiolabeled NFPs entered the axonal compartment by day 1 and achieved peak levels by 4 d (Fig. 3). Radioactivity associated with the 70-kD subunit did not decrease significantly until 17 d after injection, when the leading edge of the protein wave began its exit from the axonal window (see below). By contrast, radiolabeled forms of the 140- and 200-kD NFPs decreased ~20% ($P < 0.01$) between 4 and 17 d. Loss of this fraction of 140- and 200-kD subunits appears to reflect a pool of modified NFPs that is transported more rapidly than the main NFP wave. (25; Nixon, R. A., unpublished data). During the 3 wk after their arrival at the end of the 9-mm segment, the three [^{3}H]-NFP subunits disappeared rapidly. Beyond 45 d after injection, however, loss of the substantial population of radiolabeled neurofilament proteins still remaining in axons was more gradual.

When plotted as a logarithmic function of time, the loss of radiolabeled neurofilament proteins from the axonal window between 17 and 168 d was biphasic, with each phase exhibiting a linear rate (Fig. 4). In the first phase of disappearance between 17 and 45 d, referred to as phase I, radioactivity in each NFP subunit declined at an exponential rate ($t_{½}$ = 20–22 d). The time of initial NFP disappearance, calculated by extrapolating the first slope in Fig. 4 to 100%, occurred at 17 d for the 70-kD subunit and 12 d for the 200- and 140-kD subunits, suggesting that the leading edges of these NFP waves advanced at rates of 0.53 ± 0.3 mm/d and 0.75 ± 0.04 mm/d, respectively. Radiolabeled NFPs remaining in axons beyond 45 d (phase II), comprising ~32% of the peak radioactivity, disappeared from the axonal window with a much slower half-life ($t_{½}$ = 55 d). 6–9% of the peak radioactivity in radiolabeled NFPs was still present in axons at 168 d after synthesis. Two-dimensional electrophoretic analyses of the proteins in optic pathways at late timepoints confirmed the

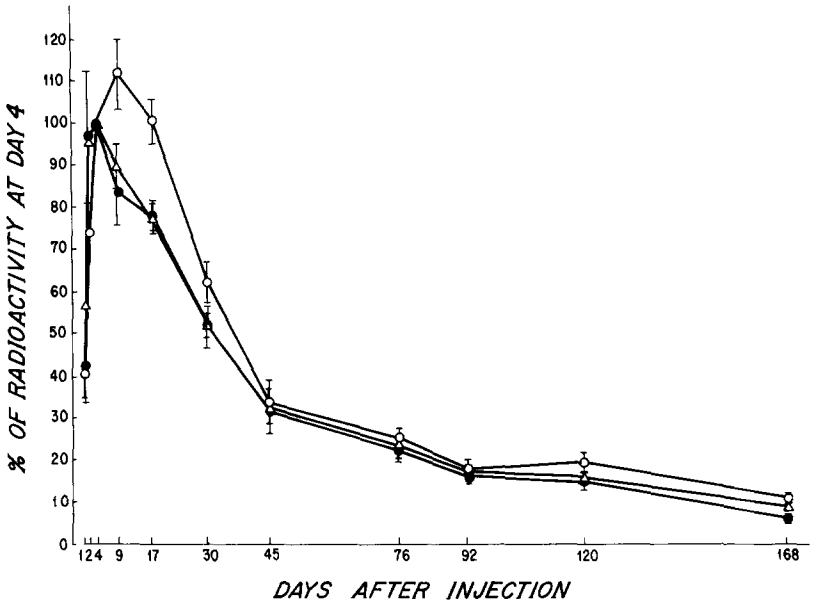

Figure 3. Relative proportions of newly synthesized NFP subunits entering and leaving a 9-mm axonal window. In each of two experiments, 80–100 mice were injected intravitreally with 25 μCi [^{3}H]proline. At different intervals after injection, optic pathways were dissected from groups of these mice. After SDS PAGE, the radioactivity associated with each NFP was quantitated and expressed as a percentage of the radioactivity present in the tissue sample at 4 d after injection. Each point is the mean ± SEM (error bars) for 7–18 determinations. The symbols indicate the three NFPs 70 kD (open circle); 140 kD (open triangle); and 200 kD (closed circle).

presence of the neurofilament triplet proteins at their characteristic positions (data not shown).

The kinetics of NFPs contrasted with the behavior of many other transported proteins, as illustrated by a major 33-kD soluble protein constituent of the SCb (group IV) phase of axoplasmic transport, referred to as protein 33 (Fig. 1). This radiolabeled protein appeared in axons earlier and disappeared more rapidly and completely than did the NFPs. Plotting the radioactivity of protein 33 as a logarithmic function of time revealed a single rate of disappearance with a half-life of 12 d (Fig. 5). The initial disappearance of this protein from the axonal window at day 4 indicated that the leading edge of this protein wave advanced at a rate of 2.00 ± 0.2 mm/d.

Distribution of Newly Synthesized NFPs along RGC Axons

To investigate the biphasic nature of NFP disappearance from axons, we studied how newly synthesized NFPs are distributed along RGC axons at intervals from 1 to 180 d after injection with [^{3}H]proline. A standard 9-mm length of the optic pathway from each mouse was divided into eight consecutive 1.1-mm segments. After pools of each segment from groups of from four to six mice were subjected to SDS PAGE, the radioactivity associated with the NFPs and other proteins was measured. At each postinjection interval, one or more electrophoretograms were fluorographed to verify that the bands identified as NFPs on stained gels corresponded to discrete radiolabeled bands (Fig. 6). These studies indicated that radioactivity in gel regions containing no discrete protein bands was lower than in NFPs. Even at the latest postinjection time points, the radioactivity associated with NFPs exceeded that in adjacent gel regions by more than 10-fold. During the first 30 d after [^{3}H]proline injection, the wavefront of radiolabeled NFPs progressed through consecutive optic pathway segments (Figs. 6 and 7, *A–C*). Linear regression analysis of changes in the position of the wavefront for six postinjection intervals between 3 and 45 d (35) revealed transport rates of 0.4–0.7 mm/d for each radiolabeled NFP. The arrival of appreciable levels of radiolabeled NFPs in distal optic pathway segments

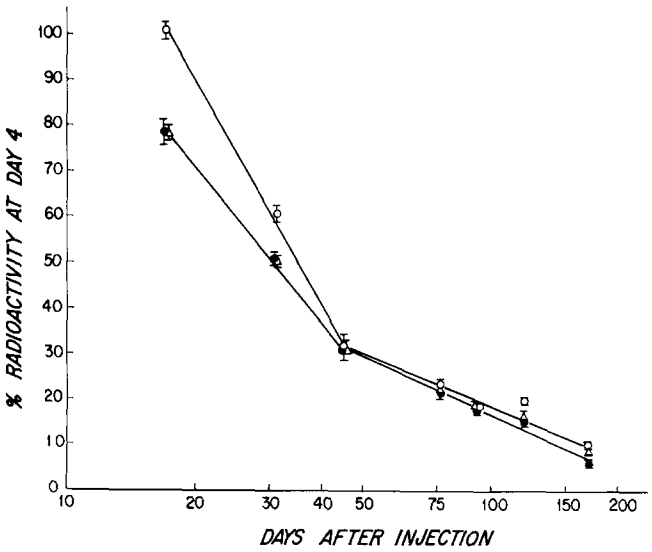

Figure 4. Biphasic disappearance of newly synthesized neurofilament proteins from RGC axons. Data presented in Fig. 3 are plotted as a logarithmic function of time (days) after injection to reveal two constant exponential rates of disappearance of radiolabeled neurofilament proteins.

coincided with the time that NFPs initially disappeared from the 9-mm axonal window in the earlier experiments (Figs. 4 and 5). By 30 d, the distribution pattern suggested that the main wave had partially exited, leaving behind a trailing portion that spanned the entire optic pathway. At this time point, segments 7 and 8 contained twofold higher levels of [^{3}H]NFPs than did the most proximal axonal sites.

In contrast to this early redistribution, little change in the distribution of radiolabeled neurofilaments persisting in axons occurred beyond 45 d (Fig. 7, *D–F*). The distribution pattern from 45 to 180 d after injection was characterized by a proximal to distal gradient of radiolabeled NFPs ranging from 6–8% (segment 1) to 16–18% (segment 8) of the total ^{3}H-NFPs in all eight segments. The stability of this distribution pattern is illustrated by the observation that the proportion of ^{3}H-NFPs in the optic nerve (segments 1–4) remained constant

at 35–40% between 45 and 180 d after injection.

The distribution analyses indicated, therefore, that disappearance of radiolabeled NFPs in phase I (Fig. 4) coincides with the exit of the SCa (group V) wave from the end of the axonal window. By contrast, NFPs leaving the axonal window in phase II, disappear at a slower constant rate by a mechanism that does not alter the distribution of these proteins along axons.

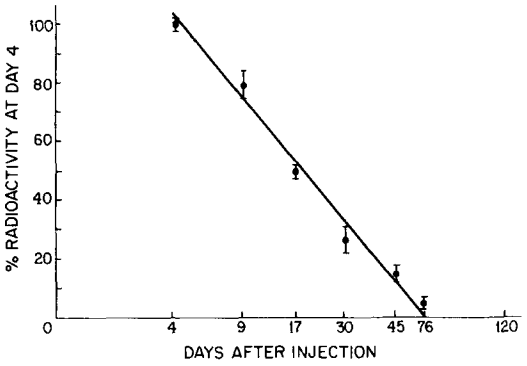

Figure 5. Disappearance of protein 33 from RGC axons after synthesis. Protein 33, a group IV (SCb) constituent, was radiolabeled as described in Fig. 2. In contrast to the kinetics of NFP loss, the rate of disappearance of this 33-kD protein (see Fig. 1) was monophasic. Each point is the mean ± SEM for 7–18 determinations.

Contribution of Delayed Perikaryal Synthesis of NFPs

Several observations indicated that retention of radiolabeled NFPs in axons is not explained by continual NFP synthesis in RGC perikarya from reused [^{3}H]proline released from retinal proteins. After intravitreal injection, [^{3}H]proline in retinal proteins reached maximal levels during the first day and gradually declined to relatively low levels during the next two months (Fig. 8). Between 4 and 17 d, the levels of ^{3}H-NFPs in axons remained relatively constant despite a loss from the retina of 4×10^6 dpm associated with other proteins. By comparison, 20% of the peak level of ^{3}H-NFPs still persisted along axons at 76 d when only 3% of the peak radioactivity in retinal proteins remained in the eye. As another example, substantial levels of ^{3}H-NFPs (15% of peak values) persisted between 76 and 120 d even though ^{3}H-labeled

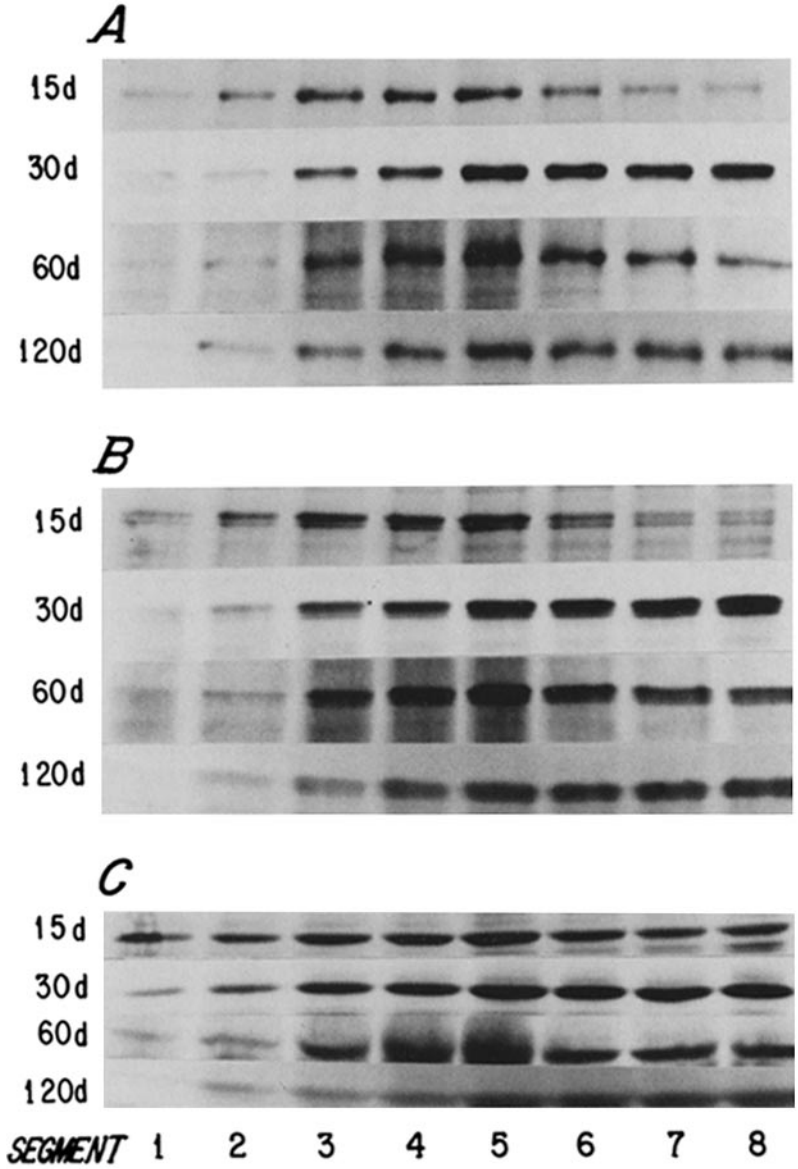

Figure 6. Distribution of radiolabeled NFPs along RGC axons at different times after synthesis. The optic pathways from mice at various intervals after intravitreal injection of [^{3}H]proline were cut into eight consecutive 1.1-mm segments extending from the eye to the lateral geniculate body. The optic nerve comprised segments 1–4; the optic chiasm is primarily contained in segment 5; and segments 6–8 are within the optic tract. Series of eight segments from groups of from six to eight mice at each postinjection timepoint were subjected to SDS PAGE and fluorography. The gel regions containing the 200-, 140-, and 70-kD NFP subunits are displayed in *A*, *B*, and *C*, respectively. The axonal distribution of the radiolabeled NFPs is shown for postinjection intervals of 15, 30, 60, and 120 d. These discrete radiolabeled bands correspond to the bands identified as NFPs in Figs. 1 and 2.

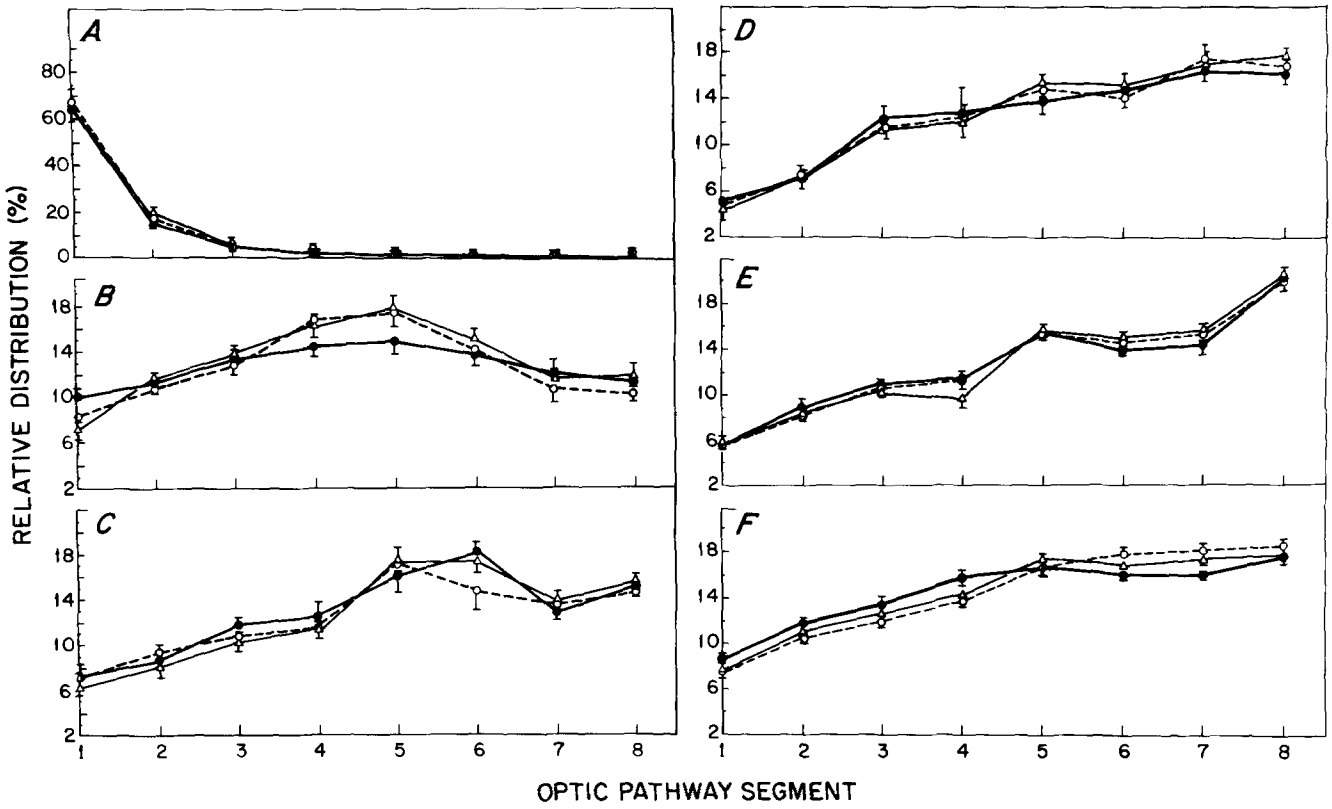

Figure 7. Quantitative distribution of radiolabeled neurofilaments along RGC axons at different times after synthesis. The optic pathways from mice at various intervals after intravitreal injection of [^{3}H]proline were cut into eight consecutive 1.1-mm segments as described in the legend of Fig. 6. Each segment was combined with corresponding segments from six to eight mice and, after SDS PAGE, radioactivity associated with NFPs was quantitated for each site along the optic pathway. The radioactivity in each neurofilament subunit at 180 d ranged from 600 to 1,700 dpm per segment. Background in the gel lane was <100 dpm. Postinjection intervals are 1 d (*A*); 15 d (*B*); 30 d (*C*); 90 d (*D*); 120 d (*E*); and 180 d (*F*). The symbols indicate the three NFPs: 70 kD (open circles); 140 kD (open triangles); 200 kD (closed circles). Each point is the average of from two to five separate experiments each involving from six to eight mice.

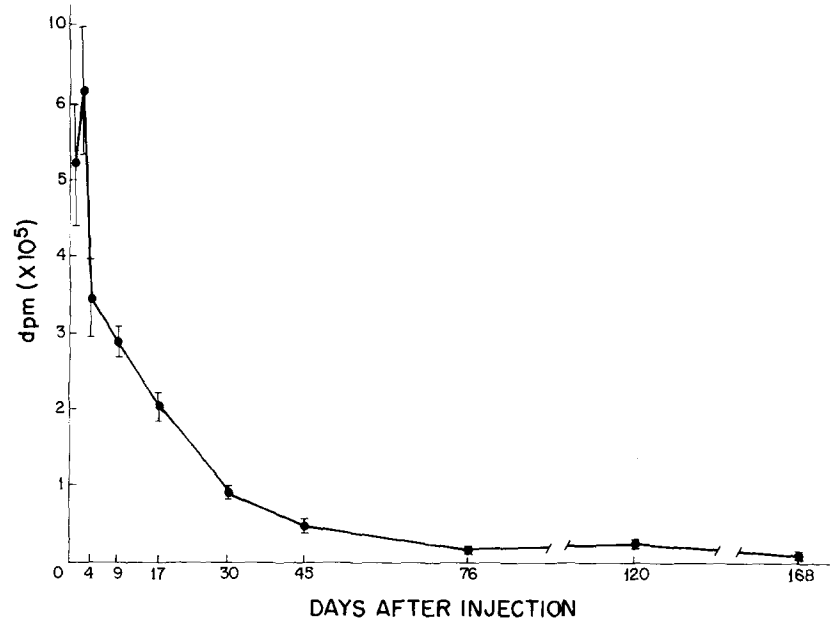

Figure 8. Disappearance of radiolabeled proteins from the retina after intravitreal injection of [^{3}H]-proline. Retinas were dissected from mice described in Fig. 3. Trichloroacetic acid–insoluble radioactivity (disintegrations per minute) was determined for each tissue sample. Each value is the mean ± SEM for the 10–20 retinal samples.

proteins in the retina did not diminish during this 44-d interval. Thus, there was little relationship between levels of radioactivity in the retina and in axonal NFPs. Furthermore, if delayed perikaryal synthesis were a significant factor, the persistance in axons of radiolabeled NFPs but only minimal amounts of various other major axonal proteins, including protein 33, would imply that released [^{3}H]proline is selectively reused for NFP synthesis. Electrophoretic analyses of retinal proteins at different postinjection intervals, however, showed that NFPs are a progressively decreasing proportion of the

total retinal protein radioactivity and that the ratio of radioactivity in protein 33 to that in NFPs increases more than threefold between 2 and 120 d in the retina. Although the radiolabeled proteins entering axons may be a small fraction of the total retinal protein, these results do not suggest that NFPs are selectively synthesized from reused amino acids.

Distribution of Total NFPs along RGC Axons

The total content of NFPs in axons reflects the steady state disposition of all NFPs entering and leaving this compartment. To examine the spatial relationship of phase I and phase II NFPs to the total NFP pool, we determined the distribution of this total pool along RGC axons. The relative amount of each neurofilament subunit in eight consecutive 1.1-mm segments of the optic nerve and tract was measured after SDS PAGE by a modified Coomassie Blue dye-binding method (33).

Each neurofilament subunit displayed a significant ($P < 0.001$) proximal to distal gradient of increasing content along the optic pathway (Fig. 9). The amount of a given neurofilament subunit was more than 2.5-fold higher in the distal optic tract than in the most proximal optic nerve segment. The total protein content was also higher distally than proximally along the optic pathway; however, these differences were smaller than the proximal to distal increases in the total content of NFPs. Expressed as a percentage of the total protein, NFPs still displayed a significant graded increase in content ($P < 0.02$). These increases are somewhat underestimated since NFPs represent a significant proportion of the total axonal protein (7). Since the ratio of NFP to total protein was lower in tissue underlying the optic tract than at any point along the optic pathway, contamination by this tissue could not explain the observed distributions.

The distribution pattern of total NFP paralleled that of newly synthesized NFPs in phase II (Fig. 9). A correlation of 0.97 ($P < 0.001$) was calculated when the total NFP content of each optic pathway segment was regressed against the radioactivity of NFPs at 120 d after injection.

Distribution of Neurofilaments along RGC Axons

If NFPs exist primarily or exclusively as stable polymers in axons (28), their distribution should parallel the spatial pattern of neurofilaments along axons. Therefore, to determine whether or not neurofilaments are present in increased numbers at distal axonal sites, morphometric analyses of neurofilament density along the length of axons were undertaken. Axonal levels at 1, 4, and 7 mm from the eye, representing proximal, middle, and distal sites of RGC axons, were examined. At each level, axons were selected randomly, but in approximately equal numbers, from each quadrant of the cross-section. The total neurofilament cross-sections per axon, the total cross-sectional area of the axon, and the total area occupied by membranous structures (i.e., vesicles, mitochondria, and agranular reticulum) were measured for each axon. The proportion of the total axonal area occupied by membranous structures was similar at proximal, middle, and distal levels of the optic pathway (5.72, 4.07, and 5.53%, respectively).

Regression analyses (Fig. 10) revealed that the number of neurofilaments was positively correlated with the total axonal area at proximal, middle, and distal axonal levels ($r = 0.90$, 0.94, and 0.94, respectively); however, the slopes and intercepts of these lines differed. The equations describing these relationships were $y = 221x - 10.289$ at 1 mm from the eye (proximal optic nerve); $y = 266x + 5.535$ at 4 mm (distal optic nerve); and $y = 311x - 2.423$ at 7 mm (distal optic tract). Comparisons of these equations indicated that the density of neurofilaments in axons (neurofilaments/total axonal cross-sectional area) increased at distal sites along the optic pathway. Neurofilament densities at the 1-mm level were significantly different from those at the 4- or 7-mm levels ($P < 0.001$). The differences among levels involved axons of all calibers; therefore, the higher neurofilament densities of axons at distal optic pathway sites did not result from a skewed selection of axons for morphometric analysis. Proximal to distal differences, however, were greater for small axons than larger ones. For example, axons with areas of <0.6 microns composed 80% of the total axonal population and ~50% of the total axonal area. In this population, neurofilament density was twofold higher at the 7-mm level than at the 1-mm level ($P < 0.001$). Neurofilament density 4 mm from the eye exhibited an intermediate value. For the total axonal popu-

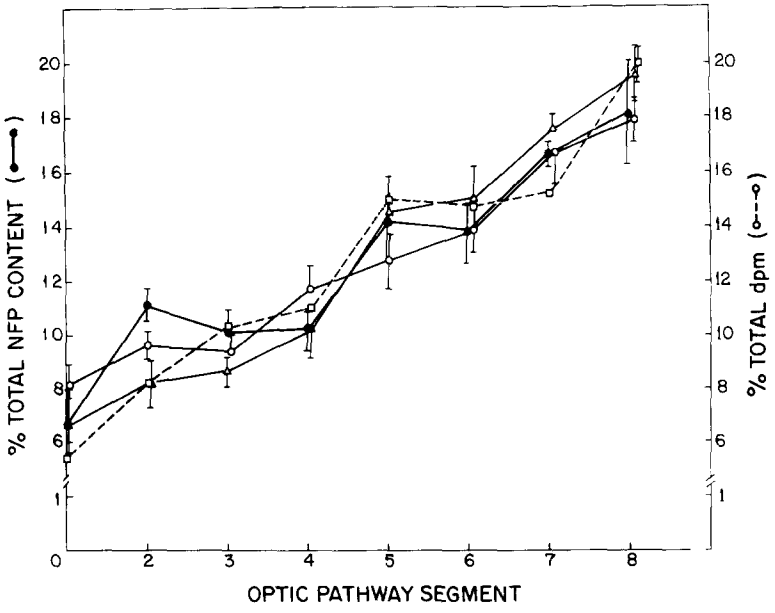

Figure 9. Distribution of NFP subunits along mouse RGC axons. Optic pathways cut into eight consecutive 1.1-mm segments as described in Fig. 6 were subjected to one-dimensional SDS PAGE. The dye-binding capacity of the three NFP subunits in each segment, which reflects relative protein content, was determined by spectrophotometry after quantitatively extracting the dye from protein bands cut from gels stained with Coomassie Brilliant Blue. Each point is the mean ± SEM for four determinations. The 200 kD (open circle), 140 kD (open triangle), and 70 kD (closed circle) NFP subunits are shown. For comparison, the dotted line (open square) indicates the total [^{3}H]-disintegrations per minute associated with the three neurofilament protein subunits at 120 d after intravitreal injection of [^{3}H]proline.

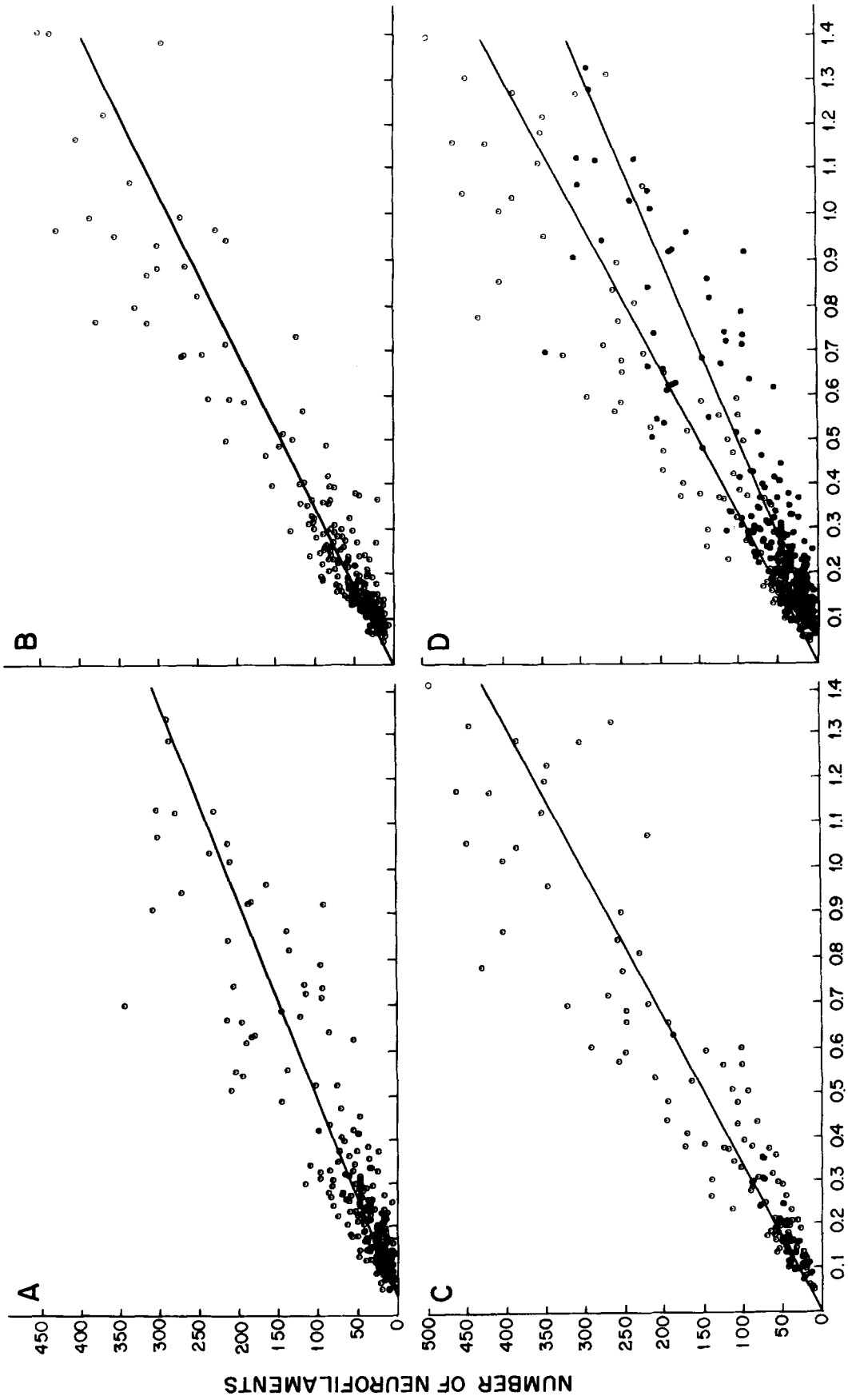

Figure 10. Relationship of the number of neurofilaments to the cross-sectional area of axons at three levels along the optic pathway. The number of neurofilaments in randomly selected axons cut in transverse section was plotted against the cross-sectional axoplasmic area in square micrometers. *A–C* depict the relationship observed at distances along the optic pathway of 1, 4, and 7 mm from the eye, respectively. *D* illustrates a comparison of the relationships seen at 1 mm (open circles) and at 7 mm (closed circles).

lation, neurofilament density at distal axonal levels was 75% higher than that at proximal sites ($P < 0.001$) and 15% higher than at middle levels ($P < 0.001$ vs. the proximal level; $P < 0.02$ vs. distal level).

Regional Variation of Axon Caliber in the Mouse Optic Pathway

Fiber number is constant along the optic nerve and only slightly higher in the optic tract than in the optic nerve as a result of commissural fibers connecting brainstem nuclei. Therefore, if the caliber of individual axons varied along their length, this would be reflected in changes in the distribution of axon calibers in the total axonal population at different levels along the optic pathway. As shown in Fig. 11, the distributions of axonal calibers in a representative portion of the total axonal population were remarkably similar at proximal, middle, and distal levels of the optic pathway. Although comparisons between proximal and distal levels revealed a barely significant difference (Kolmogorov-Smirnov test, $P < 0.05$) in the caliber distributions, the net shift was small and in the direction of increased caliber distally. The total cross-sectional area per 1,000 axons at 1 mm from the eye was 2.5% lower than that at 4 mm and 4.7% higher than that at 7 mm. These results strongly suggest that axonal caliber at different levels of individual RGC axons is relatively constant. The increased neurofilament density observed at distal axonal levels was, therefore, not due to an overall reduction in axonal calibers but rather reflected an absolute increase in neurofilament numbers. Using the equations describing the relationship between neurofilament number and axon caliber and the data on axon caliber distributions, we calculated the absolute number of neurofilaments per 100 axons to be 6,241, 9,225, and 10,208 at 1, 4, and 7 mm from the eye, respectively. This proximal to distal ratio of neurofilaments (1 to 1.75) was similar to the 1 to 1.9 ratio of total NFP content at the corresponding optic pathway levels in Fig. 9.

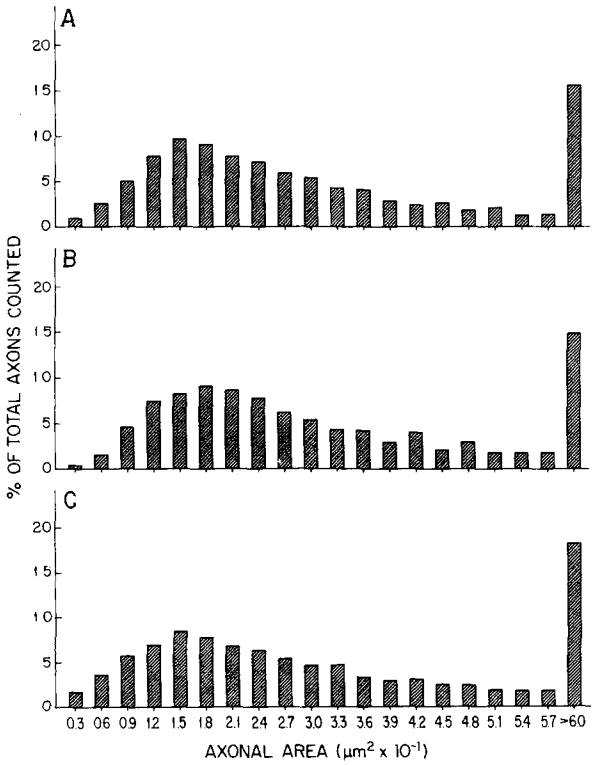

Figure 11. Distribution of axon caliber sizes at three levels along the optic pathway. These histograms compare the caliber distributions of transversely cut axons at distances along the optic pathway of 1, 4, and 7 mm from the eye. The mean number of axons in each size class, expressed as a percentage of the total, is plotted as a function of axonal diameter. About 2,700 axons were analyzed at each level in two animals.

Discussion

Moving and Stationary Pools of NFPs in RGC Neurons

Our results indicate that newly synthesized NFPs contribute to at least two pools in RGC axons, which are distinguishable by their temporal-spatial distribution along axons and kinetics of disappearance from axons. Our evidence is consistent with the notion that these two pools comprise a moving phase and a relatively stationary phase of neurofilaments and that both pools may contribute to the axonal neurofilament lattice along RGC axons.

Before they disappeared from axons, most radiolabeled proteins exhibited the characteristic time-dependent redistributions along axons that are expected of axoplasmic transport waves. The rate at which NFPs advanced, 0.5–0.7 mm/d, was similar when calculated either from movement of the leading edge of the radiolabeled wave or from the time of initial disappearance of NFPs from a 9-mm axonal window. This value is similar to rates of NFP movement within the SCa (group V) phase of axoplasmic transport that have been observed in RGC neurons of other species (1, 24, 29). Radiolabeled protein 33, by contrast, was transported at a typical SCb (group IV) rate (13, 24). Its arrival at the most distal segment of optic tract in distribution profile studies coincided with its first detectable loss from the 9-mm axonal window. The similar transport rates measured by these two approaches suggested, therefore, that the initial phase of disappearance of a protein from the axonal window (phase I) reflects movement beyond the distal limit of this window at a characteristic axoplasmic transport rate.

Protein 33 and other radiolabeled proteins (unpublished data) displayed only a single phase of disappearance. If it is assumed that this loss represents the exit of a moving wave, the exponential kinetics describe a waveform with a relatively steep advancing front and a long trailing portion that decreases gradually (Nixon, R. A., manuscript in preparation). The pattern predicted by these kinetics, therefore, resembles the observed distribution profiles of protein 33 and other SCb polypeptides (Nixon, unpublished data; 6, 13) as these proteins reach the distal end of the optic tract. The exponential disappearance rate of NFPs in phase I suggests a similar pattern; however, the shape of this waveform may be partly obscured by phase II NFPs.

A second pool of newly synthesized NFPs (phase II) was retained in axons after phase I NFPs should have been entirely eliminated from the axonal window. This time was estimated to be a maximum of 75 d based upon extrapolating curves describing the disappearance of phase I NFPs. Reuse of [^{3}H]-proline released from catabolized retinal proteins resulting in delayed export of radiolabeled NFPs from RGC perikarya could not account for either the high levels of radioactivity associated with axonal NFPs after long postinjection intervals

or the selective retention of NFPs and certain other proteins in axons.

The kinetics and axonal distribution of radiolabeled NFPs that disappear in phase II indicate that this pool constitutes a stationary or exceedingly slow-moving structure in RGC axons. The presence of appreciable levels of ^{3}H-NFPs in the proximal 1 mm portion of optic nerve 180 d after synthesis, for example, implies that these NFPs, if moving, advance at a rate that is >100-fold slower than the SCa (group V) rate of axoplasmic transport. At this rate, they would not reach synaptic terminals during the life of the animal. Entry of a fraction of newly synthesized NFPs into a stationary compartment is supported by the stability of the axonal distribution of phase II NFPs. Between 45 and 168 d after [^{3}H]proline injection, radiolabeled NFPs maintained the same nonuniform distribution along axons despite a 50% decrease in the absolute level of radioactivity associated with NFPs. By contrast, if phase II NFPs moved as a typical axoplasmic transport wave, the loss of ^{3}H-NFPs should have displayed different kinetics in proximal segments than in distal segments of the optic pathway, as observed in the case of protein 33. The nonuniform axonal distribution of neurofilaments, total NFPs, and phase II ^{3}H-NFPs represents a third line of evidence favoring a stationary component of the neurofilament lattice along axons. Under steady state conditions (implying relatively constant neurofilament proteins synthesis), a freely moving wave of protein would be expected to be uniformly distributed along axons. Although proximal to distal decreases of NFP content might arise from protein degradation, modification, or uniform deposition of neurofilaments during transport, a proximal to distal increase in steady state NFP content is difficult to explain on the basis of a change in NFP transport or metabolism. The properties of phase II NFPs and their relationship to the total NFP pool are most easily explained, therefore, by nonuniform deposition of a portion of the moving wave of NFPs into a stationary nonuniform structure along RGC axons.

Contribution of Stationary NFPs to the Axonal Cytoskeleton

The relationship of a pulse-labeled population of NFPs to the steady state level of NFPs in axons depends on two factors: the size of the newly synthesized pool and the rate of turnover or residence time of the proteins in axons, which may involve proteolysis or elimination by axoplasmic transport. The observations that radiolabeled NFPs establish a stable axonal distribution by 45 d and disappear at a constant rate suggest that this fraction, ~32% of the total pool of newly synthesized NFPs, is primarily associated with the stationary phase. This percentage may be even higher if the loss of some NFPs associated with phase II is obscured at early time points by the kinetics of phase I in Fig. 4. Provided that all NFPs are synthesized in RGC perikarya from the same precursor pool of [^{3}H]proline and thus have the same specific activity, the relative sizes of the two axonal NFP pools in the steady state may be estimated from their respective levels of radioactivity and their half-lives within axons. Since phase II NFPs turnover at least 2.75-fold more slowly than phase I NFPs, the former pool is estimated to be 1.3-fold larger in the steady state (i.e., 2.75×0.32 vs. 1.00×0.68). An even larger ratio of stationary to moving radiolabeled NFPs and a shorter half-life for phase I NFPs would be expected if the contribution of phase II to the phase I rate were subtracted. These calculations, therefore, suggest that, under steady state conditions, more NFPs in RGC axons may be relatively stationary than are associated with the pool undergoing continuous translocation by axoplasmic transport.

Turnover of the Stationary Neurofilament Network

The substantial loss of NFPs in phase II despite a stable nonuniform axonal distribution indicates that these proteins disappear at similar rates along the length of the axon. Mechanisms of turnover that are compatible with this observation include the release of radiolabeled NFPs from the stationary compartment and subsequent transport to the synapse. If ^{3}H-NFPs were slowly released in proportion to the total NFP content at each axonal site, the net redistribution of the phase II NFP pool would be small. Alternatively, a uniform turnover rate of phase II NFPs along axons could also be achieved by local proteolysis. Proteolytic enzymes with high affinity for NFPs, including calcium-activated neutral proteinases, are present along axons (30, 31, 33, 35, 36, 39, 43). One calcium-activated neutral proteinase that selectively converts the 145-kD NFPs to major 143- and 140-kD forms appears to be active along axons in vivo (35, 36). Evidence suggesting that NFPs are degraded by calcium-activated proteinases in axons undergoing Wallerian degeneration in vivo has also been reported (44). The ability of axonal proteinases to degrade NFPs in normal axons in vivo, however, is not known.

Regional Specialization of the Axonal Cytoskeleton

The observation that the density of neurofilaments varies along the axonal length adds to other evidence that the neurofilament lattice in retinal ganglion cell axons is regionally specialized. At more distal axonal levels where neurofilaments are increased in density, NFP subunits display greater chemical microheterogeneity (14, 35, 37), and certain post-translational processing mechanisms for NFPs appear to be more active, including selective limited proteolysis of the 145-kD NFPs (35) and phosphorylation (37). These interrelationships may suggest a possible role for these posttranslational modification mechanisms in the deposition or subsequent organization of newly synthesized NFPs into the stationary axonal cytoskeleton.

Molecular Form of Transported NFPs

Our evidence supports the idea that NFPs or neurofilaments are not assembled into a mature neurofilament network when they leave the RGC perikaryon but rather enter the axon either as independently moving neurofilaments or as a highly deformable structure organized by means of relatively weak interactions. The progressive broadening and trailing of the NFP wave during axoplasmic transport observed in this and other studies (see below) suggests that the association of some neurofilaments with the moving wave may be overcome by competing interactions with stationary axonal structures. As a result, these neurofilaments disengage and trail behind the wavecrest. Similar interactions have been proposed to account for the broadening of protein waves moving in other phases of axoplasmic transport (46, 48). If these interactions were extensive or of a specialized nature, the neurofilaments might then be expected to become incorporated into the stationary neurofilament lattice. This model of neurofilament transport, therefore, emphasizes that if neurofilaments are organized

into a macromolecular structure during transport, this organization must be sufficiently plastic to enable neurofilaments to leave the moving wave and interact for varying lengths of time with stationary structures. Since NFPs do not move coordinately with tubulin in mouse RGC axons (Nixon, R. A., and C. A. Marotta, manuscript in preparation), the final organization of the neurofilament-microtubule lattice probably develops only after the NFPs reach their destination in axons.

Functional Implications of Moving and Stationary Neurofilaments

Neurofilaments are believed to serve as a three-dimensional structural lattice that helps stabilize the axonal cytoplasmic matrix (22, 23, 45). If transported and relatively stationary neurofilaments participate in this function, the respective properties of these two pools may confer on the cytoskeleton somewhat different potentials for stability and plasticity. Because of its slow rate of turnover, the stationary neurofilament lattice can provide axons with a significant degree of stability even if neurofilament synthesis or transport were temporarily altered or interrupted. The presence and size of the stationary neurofilament lattice in different neurons, therefore, may define the relative permanence, as opposed to plasticity, of a given axonal shape, direction, or spatial orientation as the neuron matures. In addition, a stationary network of neurofilaments is well suited as a scaffold to organize or anchor cellular constituents into a precise topography within the axoplasm. A similar role has been suggested for intermediate filaments in certain other cell types (20, 23, 45).

Compared with the stationary neurofilament network, neurofilaments moving at slow axoplasmic transport rates represent a more rapid mechanism for modifying axonal geometry. Since moving neurofilaments are continually replaced as a function of the transport rate and length of the axon (16, 21, 31), alterations of the axonal cytoskeleton could be effected within a few weeks in most central neurons by a change in the rates of NFP synthesis or axoplasmic transport. Indeed, final axon diameter appears to be a feature of axonal shape that is determined partly by neurofilaments in the SCa wave. In axotomized and regenerating peripheral axons, increases or decreases in fiber caliber accompany changes in the delivery (synthesis or transport) of neurofilaments and occur in a seriate pattern with a time course that corresponds to the SCa rate of axoplasmic transport (16). In RGC axons, the presence of a sizable pool of continually moving neurofilaments and the high correlation between neurofilament number and axon caliber at a given level are compatible with this role for neurofilaments. The additional observation, however, that neurofilament density may vary nearly twofold along the length of an axon displaying uniform caliber suggests that other factors may also influence axon caliber in RGC neurons (11, 12, 42).

Generality of Stationary Neurofilaments—Relationship to Previous Studies

In view of these possible roles, the proportion of neurofilaments that are stationary might be expected to vary in different neuron types or at different stages of neuron maturation. Morphometric studies of axotomized peripheral motor neurons, for example, suggest that most neurofilaments may be moving at slow axoplasmic transport rates in the largest caliber axons (16, 17). Peripheral axons differ from most central axons in having much greater diameters and lengths. These or other factors are believed to be related to the possible need for a large moving phase in peripheral neurons (30). In addition, the high ratio of neurofilaments to microtubules in very large peripheral axons (17) suggests further quantitative and possibly functional differences between the neurofilament networks in these fibers and in RGC axons.

The possibility that a stationary neurofilament network in neurons is a widespread occurrence, however, does not conflict with previous observations on the axoplasmic transport of NFPs. In various neurons, cytoskeletal proteins trail behind the moving wavefront during axoplasmic transport (1, 6, 9, 29, 47, 50) and appear to be retained in axons as observed in this study; however, the existence, size, and half-life of a stationary component has not been previously investigated. If, as we suspect, the stationary neurofilament lattice is a characteristic of other neurons, the integration of transported NFPs into this structure and the dynamic balance between moving and stationary elements may be relevant to the regenerative capacity of neurons and the vulnerability of axons to degeneration in pathological states.

We are grateful to Dr. Christine Waternaux of the Mental Health Clinical Research Center (supported by NIMH grant MH 36224) at the Mailman Research Center for her assistance in carrying out the statistical analyses. We also thank Dr. Charles Marotta, McLean Hospital, for providing the neurofilament antibodies, Dr. Ursala Drager, Dept. of Neurobiology, Harvard Medical School, for supplying intermediate filament antibody, and Dr. Ronald Majocha, McLean Hospital, for assistance with immunoblot experiments. Susan Lewis, William Fisher, Donald Perlo, and Denise Hirsch provided expert technical assistance. Dr. Nixon was a Fellow of the Alfred P. Sloan Foundation during part of this study.

This research was supported by grants from the U. S. Public Health Service (NS 17535 and BRSG RR 05404) and the Anna and Seymour Gitenstein Foundation.

Received for publication 20 May 1985, and in revised form 16 October 1985.

References

1. Black, M. M., and R. J. Lasek. 1980. Slow components of axonal transport: two cytoskeletal networks. *J. Cell Biol.* 86:616–623.

2. Bradford, M. M. 1976. A rapid and sensitive method for the quantitation of microgram quantities of protein utilizing the principle of protein-dye binding. *Anal. Biochem.* 72:248–254.

3. Brown, B. A., R. E. Majocha, D. M. Staton, and C. A. Marotta. 1983. Axonal polypeptides cross-reactive with antibodies to neurofilament proteins. *J. Neurochem.* 49:299–308.

4. Brown, B. A., R. A. Nixon, and C. A. Marotta. 1982. Posttranslational processing of α-tubulin during axoplasmic transport in CNS axons. *J. Cell Biol.* 94:159–164.

5. Brown, B. A., R. A. Nixon, P. Strocchi, and C. A. Marotta. 1981. Characterization and comparison of neurofilament proteins from rat and mouse CNS. *J. Neurochem.* 36:143–153.

6. Cancalon, P. 1979. Subcellular and polypeptide distributions of slowly transported proteins in the garfish olfactory nerve. *Brain Res.* 161:115–130.

7. Chiu, F.-C., and W. T. Norton. 1982. Bulk preparation of CNS cytoskeleton and the separation of individual neurofilament protein by gel filtration: dye binding characteristics and amino acid composition. *J. Neurochem.* 39:1252–1260.

8. Draper, N. R., and H. Smith. 1966. Applied Regression Analysis. John Wiley & Sons, Inc., New York. 407 pp.

9. Filliatreau, G., and L. DiGiamberardino. 1982. Quantitative analysis of axonal transport of cytoskeletal proteins in chicken oculomotor nerve. *J. Neurochem.* 39:1033–1037.

10. Freeman, G. H., and J. H. Halton. 1951. Note on an exact treatment of contingency, goodness of fit and other problems of significance. *Biometrika.* 38:141–149.

11. Friede, R. L., and T. Samorajski. 1970. Axon caliber related to neurofilament and microtubules in sciatic nerve fibers of rats and mice. *Anat. Rec.*

167:379–388.

12. Friede, R. L., T. Miyaghishi, and K. H. Hu. 1971. Axon calibre, neurofilaments, microtubules, sheath thickness and cholesterol in cat optic nerve fibres. *J. Anat.* 108:365–373.

13. Garner, J. A., and R. J. Lasek. 1982. Cohesive axonal transport of the slow component b complex of polypeptides. *J. Neurosci.* 2:1824–1835.

14. Goldstein, M. E., L. A. Sternberger, and N. H. Sternberger. 1983. Microheterogeneity ("neurotypy") of neurofilament proteins. *Proc. Natl. Acad. Sci. USA.* 80:3101–3105.

15. Hirokawa, N., M. A. Glicksman, and M. B. Willard. 1984. Organization of mammalian neurofilament polypeptides within the neuronal cytoskeleton. *J. Cell Biol.* 98:1523–1536.

16. Hoffman, P. N., J. W. Griffin, and D. L. Price. 1984. Control of axonal caliber by neurofilament transport. *J. Cell Biol.* 99:705–714.

17. Hoffman, P. N., G. W. Thompson, J. W. Griffin, and D. L. Price. 1985. Changes in neurofilament transport coincide temporally with alterations in the caliber of axons in regenerating motor fibers. *J. Cell Biol.* 101:1332–1340.

18. Hofstein, R., R. E. Majocha, C. J. Barnstable, and C. A. Marotta. 1985. Nonuniform distribution of neurofilament epitopes in the CNS during development. *Ann. NY Acad. Sci.* 455:787–789.

19. Laemmli, U. K. 1970. Cleavage of structural proteins during the assembly of the head of bacteriophage T4. *Nature (Lond.)* 227:680–685.

20. Jones, J. C. R., A. E. Goldman, H.-Y. Yang, and R. D. Goldman. 1985. The organizational fate of intermediate filament networks in two epithelial cell types during mitosis. *J. Cell Biol.* 100:93–102.

21. Lasek, R. J., and P. N. Hoffman. 1976. The neuronal cytoskeleton, axonal transport, and axonal growth. *In* Cell Motility: Microtubules and Related Proteins. R. Goldman, T. Pollard, and J. Rosenbaum, editors. Cold Spring Harbor Laboratory, New York. 1020–1049.

22. Lasek, R. J., M. M. Oblinger, and P. F. Drake. 1984. Molecular biology of neuronal geometry: expression of neurofilament genes influences axonal diameter. *Cold Spring Harbor Symp. Quant. Biol.* 48:731–744.

23. Lazarides, E. 1982. Intermediate filaments: a chemically heterogeneous, developmentally regulated class of proteins. *Annu. Rev. Biochem.* 51:219–250.

24. Levine, J., and M. Willard. 1980. The composition and organization of axonally transported proteins in the retinal ganglion cells of the guinea pig. *Brain Res.* 194:137–154.

25. Lewis, S. E., and R. A. Nixon. 1985. Microheterogeneity of the 200,000 dalton neurofilament protein (NFP). *Trans. Am. Soc. Neurochem.* 16:245.

26. Liem, R. K. H., S.-H. Yen, G. D. Salomon, and M. L. Shelanski. 1978. Intermediate filaments in nervous tissues. *J. Cell Biol.* 79:637–645.

27. Lowry, O. H., N. J. Rosebrough, A. L. Farr, and R. J. Randall. 1951. Protein measurement with the Folin phenol reagent. *J. Biol. Chem.* 193:265–275.

28. Morris, J. R., and R. J. Lasek. 1982. Stable polymers of the axonal cytoskeleton: the axoplasmic ghost. *J. Cell Biol.* 92:192–198.

29. Mori, H., M. Komiya, and M. Kurokawa. 1979. Slowly migrating axonal polypeptides. Inequalities in their rate and amount of transport between two branches of bifurcating axons. *J. Cell Biol.* 82:174–184.

30. Nixon, R. A. 1980. Protein degradation in the mouse visual system I. Degradation of axonally transported and retinal proteins. *Brain Res.* 200:69–83.

31. Nixon, R. A. 1983. Proteolysis of neurofilaments. 1983. *In* Neurofilaments. C. A. Marotta, editor. University of Minnesota Press, Minneapolis, MN. 117–154.

32. Nixon, R. A. 1986. Fodrin degradation by calcium-activated neutral proteinase (CANP) in retinal ganglion cell neurons and optic glia: preferential localization of CANP activities in neurons. *J. Neurosci.* In press.

33. Nixon, R. A., and C. A. Marotta. 1984. Degradation of neurofilament proteins by purified human cathepsin D. *J. Neurochem.* 43:507–516.

34. Nixon, R. A., K. A. Bishop, and W. H. Fisher. 1983. Retention of axonally transported neurofilament proteins along mouse retinal ganglion cell axons. *Soc. Neurosci. Abstr.* 9:149.

35. Nixon, R. A., B. A. Brown, and C. A. Marotta. 1982. Posttranslational modification of a neurofilament protein during axoplasmic transport: implications for regional specialization of CNS axons. *J. Cell Biol.* 94:150–158.

36. Nixon, R. A., B. A. Brown, and C. A. Marotta. 1983. Limited proteolytic modification of a neurofilament protein involves a proteinase activated by endogenous levels of calcium. *Brain Res.* 275:384–388.

37. Nixon, R. A., S. E. Lewis, and C. A. Marotta. 1985. *In vivo* phosphorylation of neurofilament proteins in retinal ganglion cell (RGC) neurons. *J. Neurochem.* 44:S60.

38. Nixon, R. A., K. B. Logvinenko, and W. H. Fisher. 1985. Evidence for a stationary non-uniform network of neurofilaments along retinal ganglion cell axons. *Ann. NY Acad. Sci.* 455:797–800.

39. Nixon, R. A., R. Quackenbush, and A. Vitto. 1986. Multiple calcium-activated neutral proteinases (CANP) in mouse retinal ganglion cell neurons: specificities for endogenous neuronal substrates and comparison to purified brain CANP. *J. Neurosci.* In press.

40. O'Farrell, P. H. 1975. High resolution two-dimensional electrophoresis of proteins. *J. Biol. Chem.* 250:4007–4021.

41. Pruss, R. M., R. Mirsky, M. C. Raff, R. Thorpe, A. J. Dowding, and B. H. Anderton. 1981. All classes of intermediate filaments share a common antigenic determinant defined by a monoclonal antibody. *Cell.* 27:419–428.

42. Sasaki-Sherrington, S. E., J. R. Jacobs, and J. K. Stevens. 1984. Intracellular control of axial shape in non-uniform neurites: a serial electron microscopic analysis of organelles and microtubules in AI and II retinal amacrine neurites. *J. Cell Biol.* 98:1279–1290.

43. Schlaepfer, W. W. 1983. Neurofilaments of mammalian peripheral nerve. *In* Neurofilaments. C. A. Marotta, editor. University of Minnesota Press, Minneapolis, MN. 57–85.

44. Schlaepfer, W. W., C. Lee, J. Q. Trojanowski, and V. M.-Y. Lee. 1984. Persistence of immunoreactive neurofilament protein breakdown products in transected rat sciatic nerve. *J. Neurochem.* 43:857–864.

45. Steinert, P. M., C. R. Jonathan, R. Jones, and R. D. Goldman. 1984. Intermediate filaments. *J. Cell Biol.* 99 (1, Pt. 2):22s–27s.

46. Stewart, G. H., B. Horwitz, and G. W. Gross. 1982. A chromatographic model of axoplasmic transport. *In* Axoplasmic Transport. D. G. Weiss, editor. Springer-Verlag, Berlin. 414–422.

47. Stromska, D. P., and S. Ochs. 1981. Patterns of slow transport in sensory nerves. *J. Neurobiol.* 12:441–453.

48. Weiss, D. G., and G. W. Gross. 1982. The microstream hypothesis of axoplasmic transport: characteristics, predictions and compatibility with data. *In* Axoplasmic Transport. D. G. Weiss, editor. Springer-Verlag, Berlin. 362–383.

49. Willard, M. 1983. Neurofilaments and axonal transport. 1983. *In* Neurofilaments. C. A. Marotta, editor. University of Minnesota Press, Minneapolis, MN. 86–116.

50. Willard, M., M. Wiseman, J. Levine, and P. Skene. 1979. Axonal transport of actin in rabbit retinal ganglion cells. *J. Cell Biol.* 81:581–591.